

Combinatorial Single Particle Spectro-Microscopic Analysis of Plasmon Coupling of Gold Nanorods on Mirror


Published as part of *The Journal of Physical Chemistry virtual special issue "Nanophotonics for Chemical Imaging and Spectroscopy"*.

Seth L. Filbrun, Teng-Xiang Huang, Fei Zhao, Kuangcai Chen, Bin Dong,* and Ning Fang*

 Cite This: <https://doi.org/10.1021/acs.jpcc.1c08262>

 Read Online

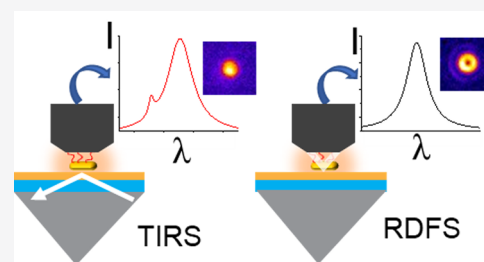
ACCESS |

 Metrics & More

 Article Recommendations

 Supporting Information

ABSTRACT: A highly correlative spectro-microscopy system was developed that combines reflected dark-field microscopy and total internal reflection scattering microscopy imaging modes with a spectrometer. This instrument facilitates the study of the particle on a mirror system by correlating the scattering images and spectra under the two different excitation schemes. Interestingly, the total internal reflection scattering microscopy reveals multiple plasmonic coupling modes that are not observed for the exact same gold nanorod in reflected dark-field microscopy. It suggests distinct plasmon coupling mechanisms for a gold nanorod on a mirror: only a single out-of-plane coupling mode is observed with reflected dark-field microscopy, while both in-plane and out-of-plane coupling modes are uncovered in total internal reflection scattering microscopy. By introducing an analyzer into the collection optics, the relative orientation of gold nanorods to the incident direction of laser beam displays large effects on the far-field scattering images and spectra.



INTRODUCTION

Plasmonic nanoparticles are significant to many researchers due to their localized surface plasmon resonance (LSPR), which confines light to a subwavelength volume and strongly enhances the near field around the particle.^{1,2} These properties result in the ability for single particle tracking, biosensing, and surface-enhanced spectroscopies.^{3,4} For example, multifunctional gold nanorods have been developed by Halas et al. to simultaneously identify and kill cancer cells via a local heating effect from the particle being excited with an infrared light source due to the LSPR of the particle.⁵ Others have focused on the near-field enhancement for surface-enhanced applications such as surface-enhanced Raman spectroscopy (SERS)⁶ and surface-enhanced fluorescence spectroscopy.⁷

Understanding the field enhancement around these nanoparticles is necessary to develop better sensors and applications with nanoparticle-based systems. To this end, many researchers have turned to particle-on-film methods to understand plasmonic enhancement between a particle and its mirror image. This method is ideal because the plasmonic interactions between a particle and its mirror image demonstrate dimer coupling in a controlled system. There have been significant efforts to study gold nanospheres on a gold film. For example, Mock et al. studied the distance dependence of nanospheres using layer-by-layer deposition of polyelectrolyte films to observe the change in the far-field scattering doughnut profile and spectroscopic blue shift with

increasing distance from the surface of the film.⁸ The effects of particle-on-film to the subnanometer level have since been studied by atomic layer deposition,⁹ DNA origami,¹⁰ and self-assembled monolayers.^{8,11,12} More recently, Horton et al. was able to recover the position of an emitter in a nanogap with the ability to localize molecules inside the nanogap with nanometer level precision.¹³ The nanoparticle–mirror gap has also been tuned via electrochemistry,¹⁴ plasmon-stimulated polymerization,¹⁵ and nanoscale oxidation.¹⁶

Gold nanorods (AuNRs) on a film have also been studied, although to a lesser extent. In one study, a single peak in the scattering spectra was observed when AuNRs were directly coupled to the gold film.¹⁷ This single peak is known as a charge transfer plasmon, which was found to be independent of the nanorod aspect ratio.¹⁸ A further study demonstrated additional plasmon coupling modes, resulting from cavity plasmons, when AuNRs were placed a few angstroms from the gold film with a dielectric spacer.¹⁹

Currently, all the studies of nanorods on a film were carried out using reflected dark-field scattering (RDFS) microscopy

Received: September 19, 2021

Revised: November 14, 2021

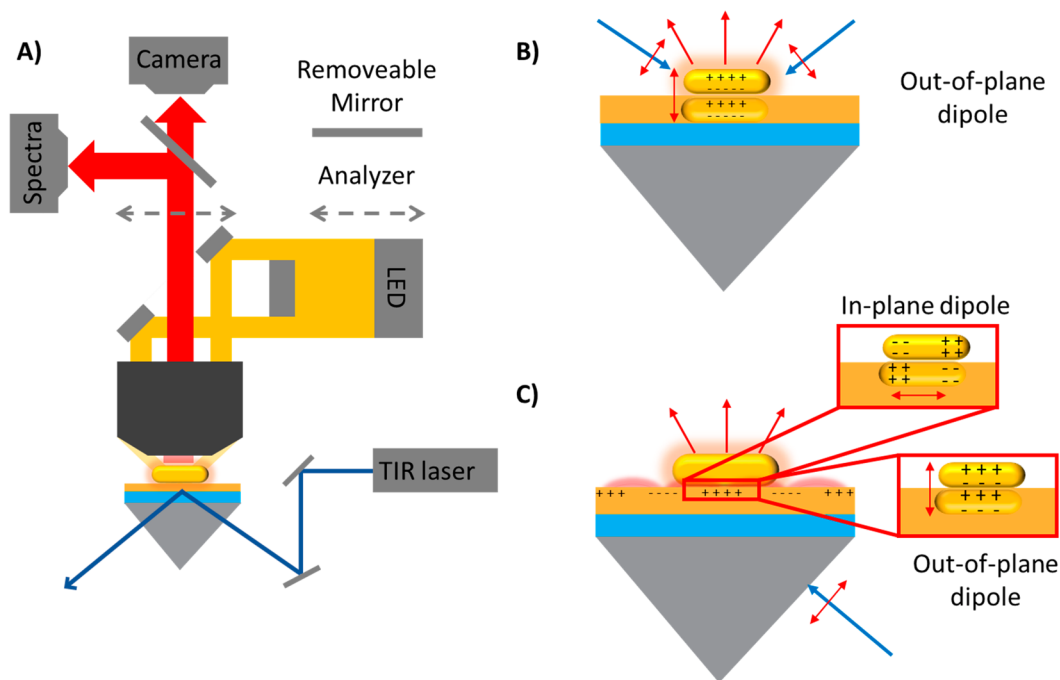


Figure 1. Schematic of the instrument set up. (A) Sample is excited with either method, and the subsequent scattering is collected through the same optics and either directed to the camera or spectrometer. (B) Reflected dark-field excitation. (C) Total internal reflection scattering microscopy with p-pol excitation.

where the particles are illuminated from the top. However, recent studies have demonstrated ultrahigh enhancement by exciting the system with extended wave surface plasmons, using a total internal reflection excitation geometry.^{20,21} Herein, we developed a combinatorial spectro-microscopy imaging system by integrating total internal reflection scattering (TIRS) microscopy and RDFS microscopy with a high-resolution spectrometer. This allows us to obtain single particle far-field scattering patterns and spectral data by exciting the plasmon coupling of AuNRs on a gold film from the top (RDFS) or with extended surface plasmons (TIRS). Using these two methods, we reveal additional plasmon coupling modes of AuNRs on a gold film are efficiently excited with TIRS, but not observable using RDFS. Furthermore, the effects of in-plane particle orientation as well as the emission polarization on the far-field scattering patterns and spectra were also investigated.

MATERIALS AND METHODS

Citrate-capped gold nanorods (40×80 nm) were purchased from Nanopartz (Loveland, CO), 50 nm gold-coated glass slides with a 2.5 nm titanium adhesion layer were purchased from Platyus Technologies (Madison, WI). Ethanol (100%) was purchased from VWR. The particles were diluted $1:10^6$ in ethanol, and 5 μ L were placed on the gold film. This gives well-separated particles for single-particle imaging (verified with scanning electron microscopy).

Total Internal Reflection (TIR). A supercontinuum laser SuperK Extreme from NKT Photonics (Birkerød, Denmark) was guided through a broad-spectrum linear polarizer and through a halfwave plate, then, through a 15 cm focusing lens before being focused onto an equilateral prism by two mirrors, the second of which is mounted on a galvanometer optical scanner (model 6220, Cambridge Technology, Cambridge MA). This mirror was mounted onto a motorized linear stage

(model MAA-PP, Newport, Irvine, CA). This allows for precise control of the laser angle into the prism. This angle is higher than the critical angle of the substrate and is adjusted slightly for each sample to the brightest intensity. See Figure S1 for a detailed instrument schematic. All optics and optomechanical components are purchased from Thorlabs (Newton, NJ), unless otherwise noted.

Reflected Dark-Field (RDF). A light-emitting diode (LED) light source (model MWWHL1, Thorlabs (Newton, NJ)) was collimated by a set of lenses and passed through a custom-made dark field stop, then to a custom-made hole mirror from Thorlabs (Newton, NJ) set at 45° angle to the incident light beam. The unpolarized light is then directed into the back focal plane of the objective and excites the sample.

Collection Optics. For the collection optics, a $100\times$ infinity corrected, 0.9 numerical aperture, reflected dark-field objective (model MPlanFLN100XBDP Olympus) was used to collect the light which was directed through an adjustable aperture and focused by tube lens with a 200 mm focal length. This light was either directed to a sCMOS camera (Dhyana 400BSI, Tucson Photonics, Fuzhou, China) to collect the far-field scattering images or a mirror was placed in the optical path (Figure S1) to direct light to the spectrometer. The spectroscopy system has an adjustable slit at the entrance of the spectrometer (Figure S1) to isolate scattering from a single particle and is equipped with an IsoPlane 160 spectrometer and a PIXIS 100B camera (Teledyne Princeton Instruments, Atton MA). RDF and TIRS images and spectra were all collected on the same particles sequentially. RDF was collected from a particle, and then TIRS was collected on the same particle. This is achieved by simply turning off the LED from RDF and turning on the laser from TIRS, allowing for true correlated measurements without moving the sample. All images were collected at a 1 s integration time, and the corresponding single particle spectra were collected at 5 s

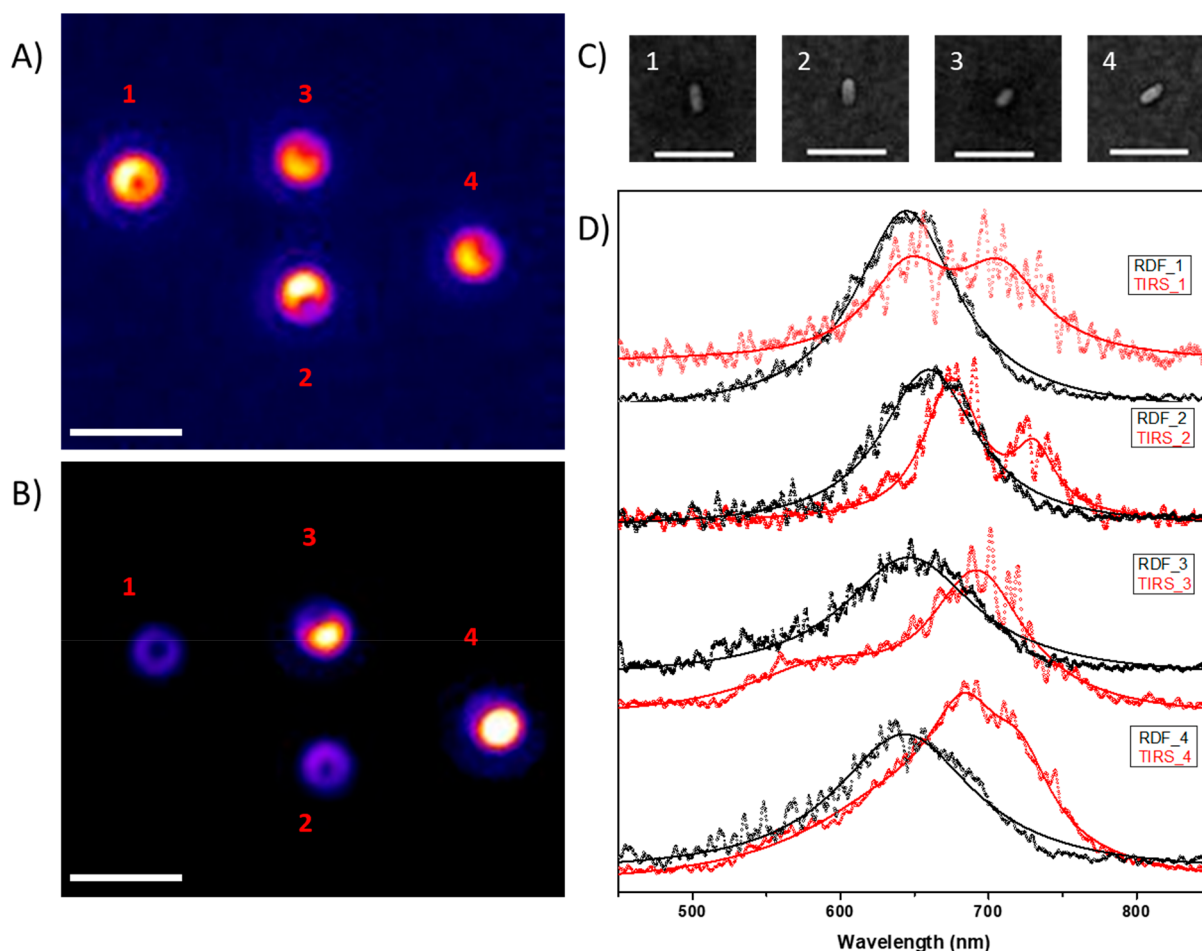


Figure 2. Correlated single particle images of gold nanorods and their corresponding spectra. (A) RDF images of gold nanorods; the numbering labels each individual particle. (B) TIRS images of the same particles in (A) showing different image patterns (scale bar $2\ \mu\text{m}$). (C) Correlative SEM images of the labeled particles (scale bar $500\ \text{nm}$) These images are cut out of the larger image shown in Figure S6. (D) Single particle scattering spectra from each particle. Black is from RDF and red is scattering from TIRS. Each spectrum was fitted with a Lorentzian function (solid line).

integration times. The collected spectra were fit with a Lorentzian function using the multiplex fit function in Origin lab. Before plotting the single particle spectra, the data were smoothed with a Savitzky–Golay filtering method to filter out some of the high frequency noise.

Scanning Electron Microscopy. The sample was mounted onto a standard aluminum stub and imaged with a secondary electron detector at $10\text{--}20\ \text{kV}$ by using a TESCAN Vega 3 scanning electron microscope at the Imaging Core Facility at Georgia State University.

RESULTS AND DISCUSSION

Spectro-Microscopy Imaging of Single AuNRs on Gold Film. The $40\ \text{nm} \times 80\ \text{nm}$ gold nanorods were first diluted in ethanol and then deposited on the surface of a thin gold film. The thin gold film was prepared atop of a glass slide by coating with a $2.5\ \text{nm}$ titanium adhesion layer and followed by $50\ \text{nm}$ of gold. The AuNRs on the gold film were prepared at a low density where they are well separated for single particle imaging. The nanorods are considered to be in direct contact with the gold film as the citrate on the surface of AuNRs will not provide sufficient electrical insulation.¹⁰ The prepared sample was then mounted on a home-designed sample stage, which enables us to illuminate the nanorods

under both reflected dark-field (RDF) and total internal reflection (TIR) configurations (Figure 1). For RDF illumination, a white color light-emitting diode (LED) light was directed through a center beam stop, allowing for a ring of light to be directed into the objective via a custom-made hole reflective mirror and focused onto the back focal plane of a $100\times$ air objective (N.A. = 0.9), as shown in Figure 1A. The sample is then illuminated at a higher angle (Figure 1B) than the collection angle of the objective ($\sim 64.3^\circ$). For TIR illumination, a supercontinuum laser was first p-polarized and focused onto the gold/air interface at an angle greater than the critical angle ($\sim 41.5^\circ$). This creates a propagating surface plasmon on the surface of the gold film, as shown in Figure 1C. The angle of the laser is fine-tuned to the TIR angle via a motorized mirror. The scattering signal from single gold nanorods under both illumination configurations (i.e., RDF scattering (RDFS) and TIR scattering (TIRS)) were collected by the same objective and analyzed by a self-built combinatorial spectro-microscopy imaging system. The switch from single particle spectroscopy analysis and single particle microscopy imaging was achieved by using a removable mirror (Figure 1A). See the Methods section for more details. The nanorod plasmon resonance is considered a polarizable electric point dipole.²² When a gold nanoparticle is placed on a gold

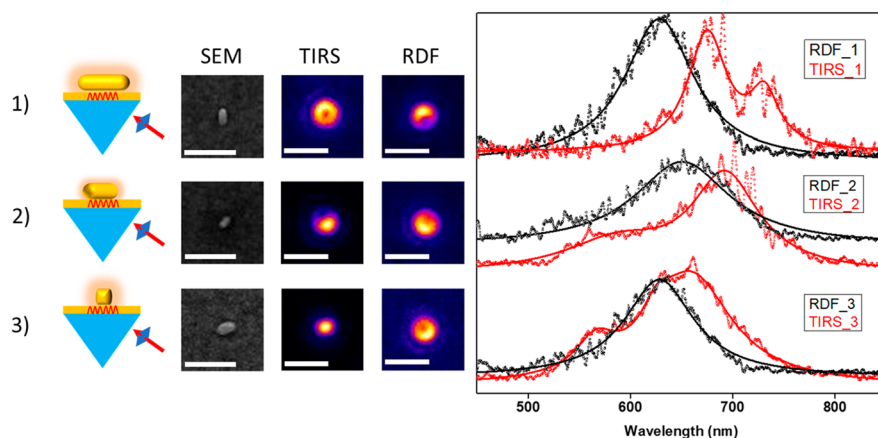


Figure 3. Particle-orientation-dependent study on the scattering patterns and spectra under RDFS and TIRS. Top row, the particle longitudinal axis is parallel to the incoming SPR wave from TIRS. Middle row is a particle approximately 45° to the incoming SPR wave. Bottom row, the particle longitudinal axis is nearly perpendicular to the incoming SPR wave from TIRS. Scale bar on optical images is $2 \mu\text{m}$ and 500 nm for the SEM images.

film, the results in dipole-image dipole coupling are synonymous with dipole–dipole interactions between two particles. This coupling interaction is either oscillating in the plane of the particle or out-of-plane of the particle. The in-plane oscillation (Figure 1C, inset) gives rise to a dot-shaped point spread function, while the out-of-plane coupling (Figure 1B) contributes to a doughnut-shaped point spread function.

Distinct Plasmon Coupling Mechanisms of a Gold Nanorod on Gold Film. Using our spectro-microscopy imaging system, we can capture both single particle scattering images and spectra with two different illumination techniques (Figure 2). Under RDF illumination, the particle images are collected, and doughnut- or half-doughnut-shaped scattering patterns are observed for the majority of single AuNRs (Figure 2A). The corresponding single particle scattering spectra are shown in Figure 2D. The single scattering peak when illuminating with RDF is indicative of charge transfer between the particle and gold film.¹⁸ For the same set of AuNRs, TIR illumination reveals vastly differing far-field scattering patterns (Figure 2B). These patterns show either doughnut-shaped (particles 1 and 2), half-doughnut shaped (particle 3), or dot-shaped (particle 4) scattering patterns. On the other hand, the TIR single particle scattering spectra for the same particles (Figure 2D) show that there is more than just one scattering peak. Depending on the particle, the peak position varies, but all the particles under TIR illumination have multiple scattering peaks. This result reveals additional plasmon-coupling modes are observed under TIR illumination. Furthermore, under TIR illumination, the single particle scattering spectra are typically red-shifted as compared to that under RDF illumination. This slight shift in peak position is most likely due to coupling between multiple modes illuminated in TIRS, which are not observable in RDF.

Upon further characterization, we found the peak position from RDF illumination is at $637 \pm 19 \text{ nm}$. When measuring the same set of AuNRs with TIR illumination, we consistently obtained multiple peaks (Figure S2); however, the peak number varied from particle to particle. Some of the particles have two peaks, and others have three or four peaks. The peak position and full width at half-maximum (fwhm) for all the particles are shown in Figure S3. The most dominant peaks that show up from TIRS are $554 \pm 20 \text{ nm}$ and $646 \pm 24 \text{ nm}$

for most particles. Two additional peaks at 686 ± 22 and $721 \pm 21 \text{ nm}$ are also observed for some particles. TIRS always gives more complex scattering spectra, but RDFS shows just one dominant peak. To further characterize the single particles using the two different illumination mechanisms, we plot the full width at half-maximum (fwhm) for each of the different peaks shown in Figure S3. The peak at 637 nm in RDF and the peak at 646 nm in TIRS, having a similar fwhm, are believed to correspond to a charge transfer, out-of-plane coupling mode.^{18,19}

These results suggest that the underlying plasmon coupling mechanisms between AuNRs and the gold film are distinctively different under these two illumination modes. In RDFS imaging, the sample is illuminated from the top where the localized surface plasmon from the particle couples with its mirror image in the gold film, then, scatters to the far field as doughnut shaped point spread function.^{8,18} This image formation is generated by out-of-plane dipole coupling between the particle and film (shown in Figure 1B).²³ It should be noted that the doughnut shaped point spread function is only observed with high NA objective lenses.^{17,24} In comparison, a propagating surface plasmon on the gold film surface is created under TIR illumination (shown in Figure 1C),^{20,21,25} which couples to the localized surface plasmon of AuNRs and generates the far field scattering images. Previous work has shown that there are multiple plasmon modes when illuminating with TIR. First, there is a dipolar coupling mode in the z -direction (similar to RDF illumination). Second, in-plane dipolar coupling occurs in the plane of the gold film that is blue-shifted to the out-of-plane mode.²⁵ We do not consider gap plasmon modes in this case since the particle is in conductive contact with the gold film.^{18,19,26} The distinct and heterogeneous scattering patterns of AuNRs in TIRS imaging as compared to that in RDFS imaging indicate more complicated plasmon coupling mechanisms than simply an out-of-plane dipole coupling.

The multiple peaks arising from TIRS excitation shown in Figure S3 are more difficult to characterize and have not been shown via dark field excitation methods. Other groups using computational methods and reflected dark field microscopy show multiple modes from nanorods when distanced from the surface of the gold film.^{26,27} It is important to note that these

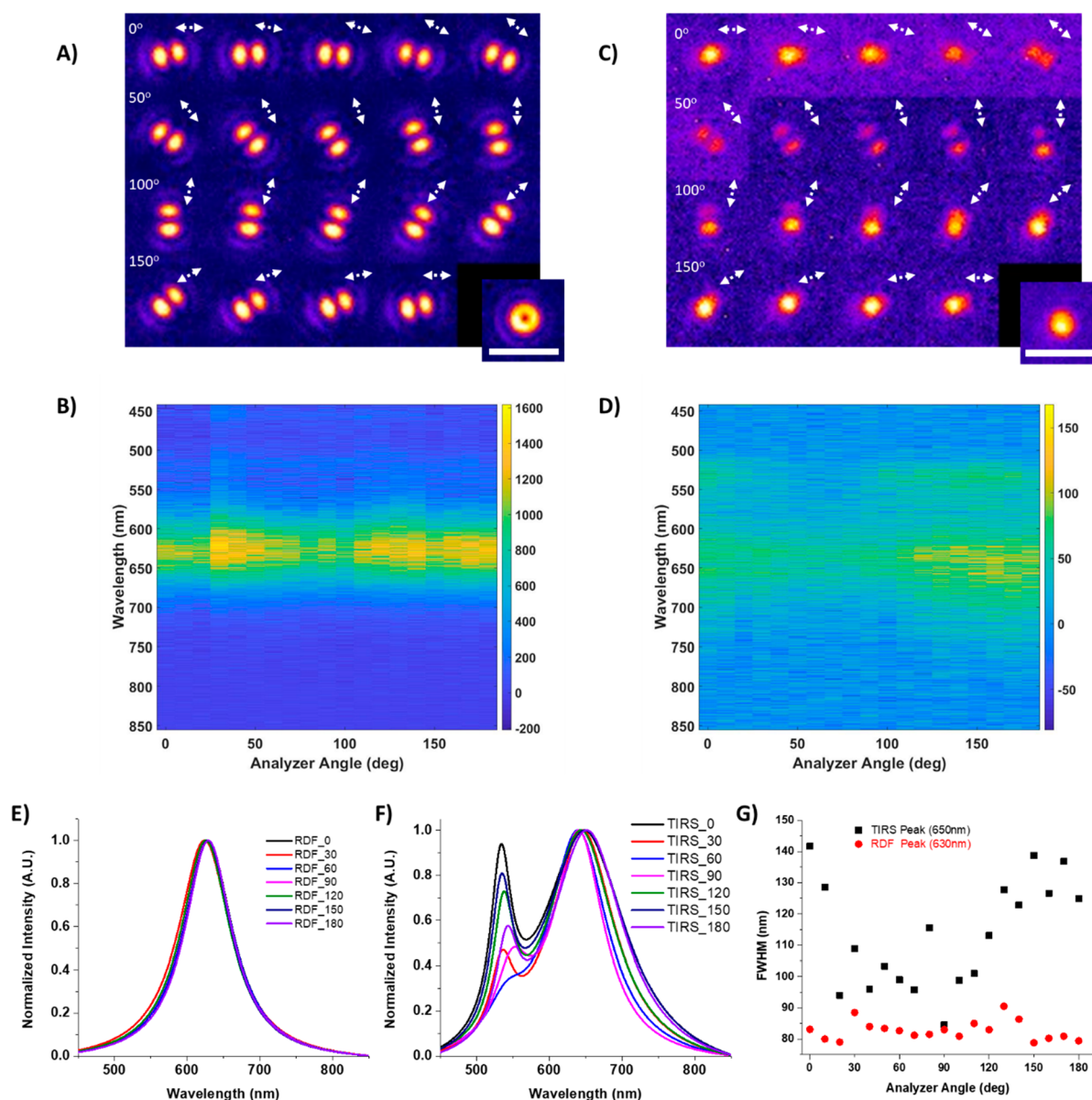


Figure 4. Polarized scattering images and spectra of the same particle using RDFS and TIRS. Images without the analyzer are shown in the offset of each of the top array (scale bar is $2\ \mu\text{m}$). The arrows represent the analyzer direction. (A, B) Images and raw scattering spectra, respectively, from RDF illumination based on different analyzer angles. (C, D) Images and raw scattering spectra from TIR illumination based on different analyzer angles. (E, F) Normalized Lorentzian fit of the RDF and TIRS peaks shown at 30° intervals. (G) The fwhm of the dominant peaks shown in (E) and (F).

papers have the nanorods separated from the gold film with a dielectric spacer. When approaching conductive contact it has been shown that multiple peaks arise,¹⁹ however, when directly in contact with the gold film, a charge transfer plasmon appears as a single peak.^{18,19} These differences demonstrate the power of combining RDFS and TIRS on the same system for highly correlated measurements.

Particle Orientation Dependent Spectro-Microscopic Properties of AuNRs on Gold Film under TIR Illumination.

AuNRs are uniformly illuminated with RDFS, but directionally illuminated with TIRS via the incoming SPR wave. Whether the orientation of anisotropic AuNRs relative to the SPR wave contribute to the complexity of scattering patterns and spectra of AuNRs on gold film in TIRS is of great interest. To correlate orientations of AuNRs with their

scattering patterns and spectra, the samples are imaged by scanning electron microscopy (SEM) where particle in-plane orientations are easily determined. Figure 3 shows spectro-microscopy imaging data of three single AuNRs with different in-plane orientations relative to the incoming SPR wave. For all three AuNRs, RDFS generates half-doughnut- or doughnut-shaped scattering patterns, as well as a single dominant spectral peak that corresponds to the out-of-plane dipole coupling from the charge-transfer mode and is independent of the in-plane particle orientation. The half-doughnut-shaped image is most likely due to the nanorod not lying completely flat on the gold film. This is because the peak position is similar, even though the image changes slightly. As seen in Figure S2A, most particles illuminated with RDF are doughnut-shaped.

On the contrary, the in-plane orientation of AuNRs affects the far-field image pattern and spectra in TIRS. Each particle has a dominant peak at ~ 650 nm which is the charge transfer mode as discussed in the previous section. When the long axis of the particle is parallel to the incoming SPR wave (Figure 3, top row), the far-field scattering pattern shows up as a donut profile and the scattering spectrum shows peaks at 670 nm (charge transfer mode) and 720 nm. See Figure S4 for the TIRS scattering with the multiple peaks shown. When the long axis of the particle is perpendicular to the incoming SPR wave (Figure 3, bottom row), the far-field scattering pattern changes to a dot shape and the scattering spectra shows peaks at ~ 550 , ~ 630 , and ~ 650 nm (charge transfer mode). When the long axis of the particle is oriented approximately 45° to the incoming SPR wave (Figure 3, middle row), the far-field scatter pattern changes to a half donut shape indicating it is somewhere in between cases of the parallel and perpendicular particles previously discussed. The corresponding TIRS spectra shows two dominant peaks, one at ~ 550 nm and the second at 670 nm. The peak at ~ 550 nm is observable when the transverse axis of the nanorod is aligned with the propagating SPR wave; thus, it corresponds to a transverse type coupling mode of the AuNRs on gold film.²⁷ These results give insights into the tunability of the in-plane coupling modes with the angle of the gold nanorod on the surface. Simulation of this coupling is needed to fully uncover the coupling origins which is beyond the scope of this paper.

Plane Polarization Decouples in-Plane versus out-of-Plane Coupling. To further understand the plane polarization of each of the coupling plasmons based on illumination direction, we placed an analyzer into the collection pathway of the microscope (dashed line in Figure 1), thus, measuring the emission polarization.²⁵ It has been shown that nanorods on a metal support emit light in a radial polarized profile.²⁸ Slices of this profile are sampled by inserting an analyzer (polarizer) into the collecting light path between the objective and tube lens. For further details, see Figure S7. We then rotated the analyzer (clockwise) in 10° increments, images and spectra were taken at each angle and displayed in Figure 4. The RDFS image shown in the inset is the unpolarized image. With the addition of the analyzer (Figure 4A), the double lobed pattern is obtained and aligned with the direction of the analyzer. The image intensity stays similar throughout the rotation. The corresponding single particle spectra (Figure 4B,E) also shows a single peak at the same position (~ 630 nm) and the peak fwhm (Figure 4G) stays consistent (~ 80 nm) throughout the entire rotation, which is consistent with the charge transfer mode excited with RDFS.

However, it is vastly different with the TIRS emission of the same particle. Figure 4C (inset) shows the unpolarized TIRS pattern. The image from TIR illumination evolves from a dot shaped pattern to a double lobed pattern as the analyzer is rotated. More insights are observable when looking at the correlated single particle TIRS spectra in Figure 4D,F. The dot-shaped image has two spectral peaks, the first one showing up at ~ 530 nm and the second at ~ 650 nm. As the analyzer is rotated, the first peak (530 nm) becomes weaker, while the second peak (650 nm) stays consistent throughout the entire rotation. This demonstrates that when illuminated with TIRS, additional coupling modes are excited and are emitting in a polarization-dependent fashion. Interestingly, the fwhm of the TIRS peak at ~ 650 nm evolves as the analyzer is rotated as well (Figure 4G), while it is constant in RDFS (~ 630 nm).

This indicates that there is one more coupling mode at a wavelength longer than 650 nm in TIRS and it is polarization-dependent as well.

The evolution of the scattering pattern and spectra with respect to the analyzer angle allows us to separate out the coupling modes. The peak that shows up at ~ 650 nm from both illumination methods is from out-of-plane coupling mode. The peaks that show up at ~ 530 and >650 nm from TIR excitation are polarizable, leading to the conclusion that they arise from in-plane coupling between the particle and the gold film. This is unique as multiple peaks from single AuNRs on gold film are only visible when exciting the particle via TIR illumination, but not RDF illumination. This technique could be used to characterize particles in the future and use TIR illumination to excite different modes that are not excited with RDFS.

Furthermore, we observed that the peak intensity changes when the analyzer is rotated with TIR illumination (Figure 4C), which arises from the polarizability of the coupling. This allows us to reveal the in-plane orientation of the AuNR by plotting the maximum intensity of the AuNR with respect to the analyzer angle. We used the maximum scattering intensity data from the images in Figure 5 and plotted them against the analyzer rotation, the data is then fitted with a $\sin^2 \theta$ function and plotted in Figure 5. When the longitudinal axis of the particle is oriented parallel to the analyzer direction, the scattering intensity measured from TIRS is the weakest.

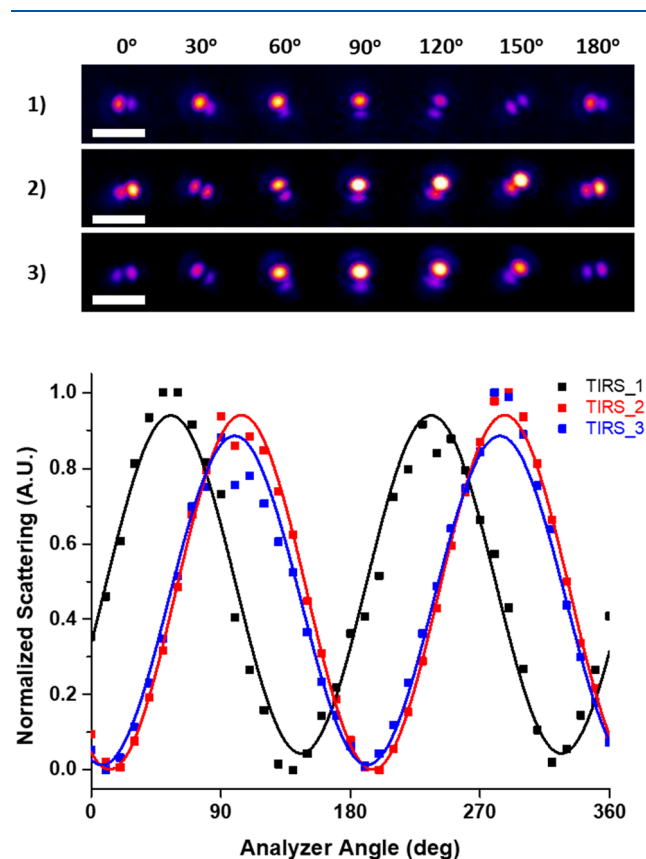


Figure 5. Image intensity data from three different particles using TIRS excitation. Maximum image intensity data recorded at each analyzer position and fit with a sine squared function. The particle images on the top row are from 30° increments. Scale bars are $2 \mu\text{m}$. (Further details can be found in the SI.)

Similarly, when the analyzer is perpendicular to the longitudinal axis of the particle the TIRS scattering intensity is the strongest. From this fitted data we can reveal the orientation of the particle without the use of correlative SEM images. The in-plane orientations of the AuNRs in Figure 5 are 145° for particle 1, 13° for particle 2, and 8° for particle 3.

CONCLUSION

In conclusion, we developed a correlative technique by realizing reflected dark field microscopy and total internal reflection scattering microscopy in the same microscope. By combining this with correlative SEM imaging, we observe image changes with TIRS relative to the incoming SPR wave which are not observable with RDFS. This is due to the underlying image formation between the particle and the film. We also observe additional scattering modes from the AuNRs on gold film when illuminated with TIR, but they are not observable when illuminating nanorods with RDF. Spectroscopic data combined with imaging reveals that in-plane dipole coupling modes are efficiently illuminated via TIRS, but are absent in RDFS. We demonstrate that the in-plane particle orientation can be determined using polarized TIRS imaging. This method of combining multiple microscopic modes with spectroscopy is useful for acquiring a more complete understanding of the particle on a mirror systems, which is essential to aid the design of plasmonic structures for enhanced performance in various applications.

ASSOCIATED CONTENT

Supporting Information

The Supporting Information is available free of charge at <https://pubs.acs.org/doi/10.1021/acs.jpcc.1c08262>.

Experimental details, additional results and discussion, and supporting figures (PDF)

AUTHOR INFORMATION

Corresponding Authors

Bin Dong – Department of Chemistry, Georgia State University, Atlanta, Georgia 30303, United States; Department of Chemistry and Biochemistry, University of Arkansas–Fayetteville, Fayetteville, Arkansas 72701, United States; Email: bind@uark.edu

Ning Fang – Department of Chemistry, Georgia State University, Atlanta, Georgia 30303, United States; The MOE Key Laboratory of Spectrochemical Analysis and Instrumentation, State Key Laboratory of Physical Chemistry of Solid Surfaces, Innovation Laboratory for Sciences and Technologies of Energy Materials of Fujian Province (IKKEM), Xiamen Key Laboratory of Analytical Molecular Nanotechnology, College of Chemistry and Chemical Engineering, Xiamen University, Xiamen, Fujian 361005, China; orcid.org/0000-0003-4710-0984; Email: nfang@xmu.edu.cn

Authors

Seth L. Filbrun – Department of Chemistry, Georgia State University, Atlanta, Georgia 30303, United States
Teng-Xiang Huang – Department of Chemistry, Georgia State University, Atlanta, Georgia 30303, United States
Fei Zhao – Department of Chemistry, Georgia State University, Atlanta, Georgia 30303, United States

Kuangcai Chen – Department of Chemistry and Imaging Core Facility, Georgia State University, Atlanta, Georgia 30303, United States; orcid.org/0000-0002-9321-9225

Complete contact information is available at: <https://pubs.acs.org/doi/10.1021/acs.jpcc.1c08262>

Notes

The authors declare no competing financial interest.

ACKNOWLEDGMENTS

This work was supported by funding from Georgia State University. N.F. acknowledges partial support from Science and Technology Projects of Innovation Laboratory for Sciences and Technologies of Energy Materials of Fujian Province (IKKEM).

REFERENCES

- (1) Sepúlveda, B.; Angelomé, P. C.; Lechuga, L. M.; Liz-Marzán, L. M. Lspr-Based Nanobiosensors. *Nano Today* **2009**, *4*, 244–251.
- (2) Maurer, T.; Adam, P.-M.; Lévêque, G. Coupling between Plasmonic Films and Nanostructures: From Basics to Applications. *Nanophotonics* **2015**, *4*, 363–382.
- (3) McNay, G.; Eustace, D.; Smith, W. E.; Faulds, K.; Graham, D. Surface-Enhanced Raman Scattering (Sers) and Surface-Enhanced Resonance Raman Scattering (Serrs): A Review of Applications. *Appl. Spectrosc.* **2011**, *65*, 825–837.
- (4) Stender, A. S.; Marchuk, K.; Liu, C.; Sander, S.; Meyer, M. W.; Smith, E. A.; Neupane, B.; Wang, G.; Li, J.; Cheng, J.-X.; et al. Single Cell Optical Imaging and Spectroscopy. *Chem. Rev.* **2013**, *113*, 2469–2527.
- (5) Hirsch, L. R.; Stafford, R. J.; Bankson, J. A.; Sershen, S. R.; Rivera, B.; Price, R. E.; Hazle, J. D.; Halas, N. J.; West, J. L. Nanoshell-Mediated near-Infrared Thermal Therapy of Tumors under Magnetic Resonance Guidance. *Proc. Natl. Acad. Sci. U. S. A.* **2003**, *100*, 13549.
- (6) Zong, C.; Xu, M.; Xu, L.-J.; Wei, T.; Ma, X.; Zheng, X.-S.; Hu, R.; Ren, B. Surface-Enhanced Raman Spectroscopy for Bioanalysis: Reliability and Challenges. *Chem. Rev.* **2018**, *118*, 4946–4980.
- (7) Dong, J.; Zhang, Z.; Zheng, H.; Sun, M. Recent Progress on Plasmon-Enhanced Fluorescence. *Nanophotonics* **2015**, *4*, 472–490.
- (8) Mock, J. J.; Hill, R. T.; Degiron, A.; Zauscher, S.; Chilkoti, A.; Smith, D. R. Distance-Dependent Plasmon Resonant Coupling between a Gold Nanoparticle and Gold Film. *Nano Lett.* **2008**, *8*, 2245–2252.
- (9) Readman, C.; de Nijs, B.; Szabó, I.; Demetriadou, A.; Greenhalgh, R.; Durkan, C.; Rosta, E.; Scherman, O. A.; Baumberg, J. J. Anomalous Large Spectral Shifts near the Quantum Tunnelling Limit in Plasmonic Rulers with Subatomic Resolution. *Nano Lett.* **2019**, *19*, 2051–2058.
- (10) Chikkaraddy, R.; Turek, V. A.; Kongsuwan, N.; Benz, F.; Carnegie, C.; van de Goor, T.; de Nijs, B.; Demetriadou, A.; Hess, O.; Keyser, U. F.; et al. Mapping Nanoscale Hotspots with Single-Molecule Emitters Assembled into Plasmonic Nanocavities Using DNA Origami. *Nano Lett.* **2018**, *18*, 405–411.
- (11) Ciraci, C.; Hill, R. T.; Mock, J. J.; Urzhumov, Y.; Fernández-Domínguez, A. I.; Maier, S. A.; Pendry, J. B.; Chilkoti, A.; Smith, D. R. Probing the Ultimate Limits of Plasmonic Enhancement. *Science* **2012**, *337*, 1072–1074.
- (12) Hill, R. T.; Mock, J. J.; Hucknall, A.; Wolter, S. D.; Jokerst, N. M.; Smith, D. R.; Chilkoti, A. Plasmon Ruler with Angstrom Length Resolution. *ACS Nano* **2012**, *6*, 9237–9246.
- (13) Horton, M. J.; Ojambati, O. S.; Chikkaraddy, R.; Deacon, W. M.; Kongsuwan, N.; Demetriadou, A.; Hess, O.; Baumberg, J. J. Nanoscopy through a Plasmonic Nanolens. *Proc. Natl. Acad. Sci. U. S. A.* **2020**, *117*, 2275–2281.
- (14) Mock, J. J.; Hill, R. T.; Tsai, Y.-J.; Chilkoti, A.; Smith, D. R. Probing Dynamically Tunable Localized Surface Plasmon Resonances

of Film-Coupled Nanoparticles by Evanescent Wave Excitation. *Nano Lett.* **2012**, *12*, 1757–1764.

(15) Ding, T.; Mertens, J.; Lombardi, A.; Scherman, O. A.; Baumberg, J. J. Light-Directed Tuning of Plasmon Resonances Via Plasmon-Induced Polymerization Using Hot Electrons. *ACS Photonics* **2017**, *4*, 1453–1458.

(16) Ding, T.; Sigle, D.; Zhang, L.; Mertens, J.; de Nijs, B.; Baumberg, J. Controllable Tuning Plasmonic Coupling with Nano-scale Oxidation. *ACS Nano* **2015**, *9*, 6110–6118.

(17) Chen, X.; Yang, Y.; Chen, Y.-H.; Qiu, M.; Blaikie, R. J.; Ding, B. Probing Plasmonic Gap Resonances between Gold Nanorods and a Metallic Surface. *J. Phys. Chem. C* **2015**, *119*, 18627–18634.

(18) Kafle, B.; Gieri, P.; Kookhaee, H.; Tesema, T. E.; Haq, S.; Manjavacas, A.; Habteyes, T. G. Robust Charge Transfer Plasmons in Metallic Particle–Film Systems. *ACS Photonics* **2018**, *5*, 4022–4029.

(19) Haq, S.; Tesema, T. E.; Patra, B.; Gomez, E.; Habteyes, T. G. Tuning Plasmonic Coupling from Capacitive to Conductive Regimes Via Atomic Control of Dielectric Spacing. *ACS Photonics* **2020**, *7*, 622–629.

(20) Abdulhalim, I. Coupling Configurations between Extended Surface Electromagnetic Waves and Localized Surface Plasmons for Ultrahigh Field Enhancement. *Nanophotonics* **2018**, *7*, 1891–1916.

(21) Li, A.; Isaacs, S.; Abdulhalim, I.; Li, S. Ultrahigh Enhancement of Electromagnetic Fields by Exciting Localized with Extended Surface Plasmons. *J. Phys. Chem. C* **2015**, *119*, 19382–19389.

(22) Li, G.-C.; Zhang, Q.; Maier, S. A.; Lei, D. Plasmonic Particle-on-Film Nanocavities: A Versatile Platform for Plasmon-Enhanced Spectroscopy and Photochemistry. *Nanophotonics* **2018**, *7*, 1865–1889.

(23) Baumberg, J. J.; Aizpurua, J.; Mikkelsen, M. H.; Smith, D. R. Extreme Nanophotonics from Ultrathin Metallic Gaps. *Nat. Mater.* **2019**, *18*, 668–678.

(24) Chikkaraddy, R.; Zheng, X.; Benz, F.; Brooks, L. J.; de Nijs, B.; Carnegie, C.; Kleemann, M.-E.; Mertens, J.; Bowman, R. W.; Vandenbosch, G. A. E.; et al. How Ultranarrow Gap Symmetries Control Plasmonic Nanocavity Modes: From Cubes to Spheres in the Nanoparticle-on-Mirror. *ACS Photonics* **2017**, *4*, 469–475.

(25) Chen, J.-D.; Xiang, J.; Jiang, S.; Dai, Q.-F.; Tie, S.-L.; Lan, S. Radiation of the High-Order Plasmonic Modes of Large Gold Nanospheres Excited by Surface Plasmon Polaritons. *Nanoscale* **2018**, *10*, 9153–9163.

(26) Sugimoto, H.; Yashima, S.; Fujii, M. Hybridized Plasmonic Gap Mode of Gold Nanorod on Mirror Nanoantenna for Spectrally Tailored Fluorescence Enhancement. *ACS Photonics* **2018**, *5*, 3421–3427.

(27) Huang, S.; Ming, T.; Lin, Y.; Ling, X.; Ruan, Q.; Palacios, T.; Wang, J.; Dresselhaus, M.; Kong, J. Ultrasmall Mode Volumes in Plasmonic Cavities of Nanoparticle-on-Mirror Structures. *Small* **2016**, *12*, 5190–5199.

(28) Zhuo, X.; Yip, H. K.; Ruan, Q.; Zhang, T.; Zhu, X.; Wang, J.; Lin, H.-Q.; Xu, J.-B.; Yang, Z. Broadside Nanoantennas Made of Single Silver Nanorods. *ACS Nano* **2018**, *12*, 1720–1731.